SCC Report 87 - 03

4

SEVERN COMMUNICATIONS CORPORATION

Satellite Observation Of Atmospheric Nuclear Gamma Radiation

31 August 1987

SEVERN COMMUNICATIONS CORPORATION
Box 544
Severna Park, Maryland 21146

Report Documentation Page

Report: SCC 87-03

Date: 31 August 1987

Title: Satellite Observation of Atmospheric Nuclear Gamma Radiation

Authors: John R. Letaw
Severn Communications Corporation
Severna Park, MD 21146

G.H. Share, R.L. Kinzer, and R. Silberberg
E.O. Hulburt Center for Space Research
Naval Research Laboratory, Washington, DC 20375

E.L. Chupp and D.J. Forrest
Department of Physics
University of New Hampshire, Durham, NH 03824

E. Rieger
Institut fur Extraterrestriche Physik
Max Planck Institut fur Physik und Astrophysik
Garching, Federal Republic of Germany

Contract: #N00014-87-C-2251
Naval Research Laboratory
4555 Overlook Avenue, S.W.
Washington, DC 20375

Abstract: A satellite observation of the spectrum of atmospheric gamma ray lines between 300 keV and 8.5 MeV is presented. The data were collected by the Gamma Ray Spectrometer on the Solar Maximum Mission between 1980 and 1983. 20 atmospheric gamma ray lines are identified with unprecedented statistical accuracy.

SATELLITE OBSERVATION

OF

ATMOSPHERIC NUCLEAR GAMMA RADIATION

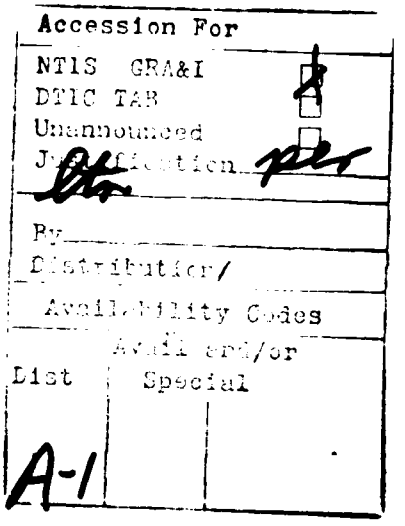

John R. Letaw
Severn Communications Corporation
Severna Park, Maryland 21146

G.H. Share, R.L. Kinzer, and R. Silberberg
E.O. Hulburt Center for Space Research
Naval Research Laboratory, Washington, D.C. 20375

E.L. Chupp and D.J. Forrest
Department of Physics
University of New Hampshire, Durham, New Hampshire 03824

E. Rieger
Institut fur Extraterrestriche Physik
Max Planck Institut fur Physik und Astrophysik, Garching, FRG

ABSTRACT

We present a satellite observation of the spectrum of gamma radiation from the Earth's atmosphere in the energy interval from 300 keV to 8.5 MeV. The data were accumulated by the Gamma Ray Spectrometer on the Solar Maximum Mission over three and one-half years, from 1980 to 1983. The excellent statistical accuracy of the data allows 20 atmospheric line features to be identified. Many of these features contain a blend of more than one nuclear line. All of the lines (with the exception of the 511 keV annihilation line) are Doppler broadened. Line energies and intensities are consistent with production by secondary neutrons interacting with atmospheric ^{14}N and ^{16}O. Although we find no evidence for other production mechanisms, we cannot rule out significant contributions from direct excitation or spallation by primary cosmic-ray protons. The relative intensities of the observed line features are in fair agreement with theoretical models; however, existing models are limited by the availability of neutron cross sections, especially at high energies. The intensity and spectrum of photons at energies below the 511 keV line, above a power-law continuum, can be explained by Compton scattering of the annihilation line photons in traversing an average of ~ 21 g cm^{-2} of atmosphere.

INTRODUCTION

Among astrophysical sources of gamma radiation, the Earth is by far the most intense object observed by satellite-borne spectrometers. Cosmic radiation traversing the upper atmosphere is responsible for a complex series of interactions ultimately leading to a gamma-ray albedo. This radiation is a source of background for satellite and balloon-borne gamma-ray telescopes. An understanding of atmospheric gamma rays and their effects on instruments can improve the sensitivities of telescopes, for example, those on NASA's Gamma Ray Observatory. The presence of intense lines with energies $E \geq 1$ MeV provides the opportunity for in-flight detector calibration.

The atmospheric gamma-ray spectrum also provides information on the production of neutron and proton-induced gamma-ray lines in a complex medium. Most of the critical parameters, such as molecular composition of the atmosphere, particle fluxes, and geometry are well known. Thus extensive tests of our understanding of complex transport processes can be made. Improvements in our knowledge of less well-known transport factors, such as neutron cross sections, may also be possible by studying the atmospheric spectrum. Measurements of this spectrum also provide an opportunity for testing particle interaction models of gamma-ray line production at the sun, the planets, and other astrophysical sources.

The atmospheric gamma-ray spectrum has been observed previously on several occasions. Peterson, Schwartz, and Ling [1973] (PSL) reported a balloon measurement of the atmospheric background spectrum below 10 MeV. Their measurements clearly reveal the 511 keV line due to annihilation of positrons produced in air showers and from β-decay of radioactive nuclei. The most detailed study to date of the positron annihilation line at 511 keV was made using the HEAO-3 germanium spectrometer [Mahoney, Ling, and Jacobson, 1981; see also references therein for other studies]. The remainder of the spectrum (above 1 MeV) was described by PSL as a "steep and relatively structureless continuum." The continuum was represented as a power law ($dN/dE \propto E^{-\alpha}$ counts s^{-1} MeV^{-1}) with spectral index $\alpha = 1.4$. Measurements of the spectral index of the upward-moving atmospheric background in the range 2 to 20 MeV [e.g. Ryan et al., 1977 and Lockwood et al. 1979] are consistent with PSL's isotropic measurement.

Measurements with improved sensitivity and energy resolution resolved some specific line features above 1 MeV. Ling [1975] summarized some of these early measurements of the 2.31 MeV line from ^{14}N, the 4.44 MeV lines from ^{12}C and ^{11}B, the 6.1 MeV line from ^{16}O, and the line complex at about 6.7 MeV. More detailed measurements of these high-energy atmospheric line features have been reported by Willett et al. [1979] and Dunphy et al. [1981]

In this paper we present observations and analysis of the atmospheric gamma-ray albedo in the range from 300 keV to 8.5 MeV. The data were collected by the gamma-ray spectrometer on the Solar

Maximum Mission (SMM) satellite over the period from 1980 February 1980 through 1983 September. During this time, the spectrometer always pointed within ~10° of the Sun and therefore viewed the Earth during approximately half of its orbit. Data accumulated over 1.5 x 10^6 s of detector live-time with unprecedented statistical significance has been obtained. Raw spectra consist of lines and continua from both the atmospheric and radioactive materials produced in the detector and spacecraft. Our analysis of this data set reveals about 20 atmospheric gamma-ray line features (at varying levels of significance), most of which have not been observed before.

INSTRUMENT

NASA's Solar Maximum Mission Satellite (SMM) was launched on 1980 February 14. The gamma-ray spectrometer (GRS) is one of seven instruments designed to study the sun over a broad spectral range from the visual to energies ~100 MeV. A drawing of the GRS is shown in Figure 1. It consists of seven cylindrical 7.5 cm x 7.5 cm NaI scintillation detectors, shielded by a 2.5 cm thick CsI annulus and a 7.5 cm CsI back plate which define a broad aperture of ~ 120° full width at half maximum (FWHM) at 511 keV [Forrest et al., 1980]. The 7 detectors are actively gain stabilized; their outputs are summed to register the total energy loss of gamma-ray events unaccompanied by a signal indicating an interaction in the CsI shields or plastic scintillation detectors, which complete the 4π anticoincidence shield for charged particles. Spectra are accumulated each 16.38 s in 476 channels covering the range from ~ 300 keV to ~ 9 MeV.

The active gain control has performed flawlessly and permits spectra accumulated over tens of months to be summed without degradation in resolution (7% FWHM at 662 keV). This capability has made possible the detection of the interstellar ^{26}Al line [Share et al., 1985] and the 511 keV annihilation line [Share et al., 1987]. As we discuss below, it also allows atmospheric lines to be measured with unprecedented statistical precision.

DATA SET AND DATA ANALYSIS PROCEDURE

The data set analyzed in this paper was collected over the period from 1980 February through 1983 September. Spectrum (a) plotted in Figure 2 is the count spectrum accumulated over this time interval while the center of the Earth was within 36° of the detector axis and the vertical rigidity cutoff was less than 11 GV/c. Under these conditions the intensity of the atmospheric lines relative to the instrumental lines is greatest. To further reduce the radioactive instrumental background the data set is restricted to periods more than 10^4 s after the last significant South Atlantic Anomaly passage.

The observed count spectrum plotted in Figure 2(a) contains both intrinsic background lines, from radioactivity induced by energetic-particle interactions in the detector and spacecraft, and gamma radiation emitted from the atmosphere. The intense lines at 1.17 MeV and 1.33 MeV are leakage from a ^{60}Co gain stabilization source within the detector. Other lines from the decay of spallation products of sodium, iodine, cesium, iron, and nickel within the instrument are also visible. A discussion concerning the identification of these instrumental lines can be found in Share et al. [1987]. Atmospheric lines at 511 keV and 4.44 MeV (from ^{11}B or ^{12}C) are also prominent in the count spectrum. They are the strongest features of atmospheric origin.

The contribution of the instrumental background to spectrum (a) shown in Figure 2 can be reduced significantly by subtracting a spectrum accumulated under the same conditions, but with the detector pointing at an angle > 144° from the center of the Earth. This procedure also reduces the measured atmospheric line intensities above 1 MeV in the subtracted spectrum by about 50%, because atmospheric gamma rays leak through the CsI shields into the detector when it is pointing away from the earth. The 511 keV line is reduced by about 25%. The 'earth-pointing' minus 'sky-pointing' spectrum is shown as spectrum (b) in Figure 2. The ^{60}Co calibration lines and other internal background features are essentially eliminated by this subtraction. Residual intensities of intrinsic background lines are about 1% of their intensity in the raw count spectrum. Any celestial lines would appear as negative features in the difference spectrum; however, the atmospheric intensity is expected to be at least an order of magnitude greater.

The resulting difference spectrum, attributed to atmospheric photons, is shown in detail in Figure 3 through Figure 7. The most significant features in this spectrum appear at about 0.511, 4.4, and 6.2 MeV. Several other line features are also apparent. The statistical significance of the data is excellent, as indicated by plotted uncertainties. About 10^8 atmospheric photons are accumulated in the plotted spectrum. Limiting errors in the analysis which follows are therefore systematic.

The primary task in analyzing the atmospheric spectrum displayed in Figure 3 through Figure 7 is the determination of the energy, intensity, and width of the many overlapping lines evident in the figures. There is a substantial amount of information in the spectrum and several steps of analysis are required to extract it. The overall procedure is outlined here and detailed in subsequent paragraphs. We first estimated the parameters associated with the underlying continuum, identified the line features, and obtained their relative intensities using manual techniques. We then utilized a non-linear least squares fitting program, including the instrument's response function, to obtain more precise estimates the line characteristics. Final manual adjustments were made to improve the overall fit to the data.

Each step in the analysis began with a model of the photon spectrum incident on the detector. The model is composed of a power-law continuum with an arbitrary number of Gaussian lines superimposed. The model photon spectrum was folded through the instrument response matrix to produce the expected count spectrum observed in the instrument. This response matrix was derived from both detector calibrations and Monte Carlo simulations, and has been applied to the analysis of solar gamma-ray spectra [Murphy, 1985]. The matrix contains channel energy and width assignments, accounts for Compton scattering and escape peaks, and corrects for detector non-linearities. Comparison of the expected count spectrum within the detector with the observed spectrum is facilitated by the χ^2 test.

Our model imposes some limitations on the observational results. The restriction to Gaussian-shaped lines is not strictly correct. Line blending and Doppler broadening are expected to cause variable line shapes. No attempt has been made to decompose strongly blended lines into individual constituents or to model the structure of Doppler-broadened lines. Both efforts depend on our currently inadequate understanding of gamma-ray line production mechanisms within the atmosphere. Furthermore, a power-law function may only approximate the atmospheric continuum. Deviations from a pure power law will be reflected as systematic errors in the measured line parameters.

Initial parameters of the underlying power law continuum were obtained by fitting this functional form to data in the ranges 0.9 to 1.0 MeV and 7.5 to 8.5 MeV where strong atmospheric line features are neither observed nor expected. In later fitting steps, the parameters of this continuum spectrum were allowed to vary along with the line parameters.

THE FIT TO THE ATMOSPHERIC SPECTRUM

The spectral analysis discussed in the previous section was applied to the spectral band shown in Figure 3 through Figure 7. The curves superimposed over the count spectra in these figures are our best fit to the data for a model containing an underlying power-law continuum and Gaussian-shaped lines. In this section we present the best-fit parameters, and discuss the goodness of fit and limitations of the model.

The Fitted Parameters

The continuum background underlying the line contributions from the atmosphere was modeled as a single power law of the form $dN_\gamma/dE = AE^{-\beta}$ photons s^{-1} MeV^{-1}. The spectral index, β, is 1.16. This was derived from the power-law index of $\alpha = 1.63$ observed in the count spectrum from the detector.

The parameters of the 20 Gaussian line features and their uncertainties are presented in Table 1. These parameters are the center energy, relative intensity, and intrinsic width (the instrumental resolution has been removed). Care must be taken in comparing these values with absolute intensities of the line features. The angular dependence of the atmospheric emission and the detector's angular response have not been unfolded from the measurements; therefore these values only approximate the absolute disk average

intensity. Corrections for leakage of the atmospheric lines into the 'sky-viewing' spectrum used to remove the instrumental background lines from the 'earth-viewing' spectrum have also not been included. These corrections are energy dependent and are estimated to be ~ 25% at 511 keV and ~ 50% between 1 MeV and 8.5 MeV. We also remind the reader that these parameters were derived under the assumption that our relatively simple model is valid. There are certain features that are not fitted properly; these are identified in the Table.

Goodness of Fit

While this model appears to provide a good fit to the data, the overall χ^2/DOF for the fit over the interval 1.5 MeV to 8.5 MeV is 2.4. The value of χ^2/DOF is even less satisfactory at lower energies as described below. We have been unable to improve the fit within the confines of our spectrum and detector models. Probable reasons for this are:

(1) Statistics are so good within this data set that changes in the number of counts from bin to bin are often much greater than the statistical uncertainty in a given bin. In this case, the midpoint of the bin is not a good approximation to the mean energy deposited by photons appearing in that bin. This problem is at its worst at low energies where statistics are best. (For example, our best fit to the 511 keV line discussed below has χ^2/DOF of about 60 even after corrections have been made for Compton scattering in the atmosphere.)

(2) Our knowledge of detector response, as represented by the response matrix, is based on calibrations involving fewer counts per channel than contained in the accumulated atmospheric spectrum. Variations of 2 or 3 standard deviations in the number of counts in adjacent channels are common. Such variations indicate the presence of differential non-linearity in the pulse height analyzer which has not been corrected. After smoothing the data so that the number of counts in each channel is averaged with its two neighbors, we obtain a value for χ^2/DOF of 1.0 over the interval 1.5 MeV to 8.5 MeV. This suggests that assignment of individual channel widths may be in error by a few percent; an amount which is consistent with the design specifications of the instrument.

Limitations of the Model

In addition to deficiencies in the global fit discussed above, the fit shows imperfections in some localized spectral regions which are apparent in the Figures.

Our assumption that a simple power law can represent the underlying continuum may force the algorithm to fit improperly the shape, energy, and intensity of some weaker line features. Some of these regions are discussed in detail in the next Section (e.g., the line features at 2.78 and 3.02 MeV). For this reason, the reader is cautioned that the parameters listed in Table 1 are the best fits

obtained from the model; in certain instances the values and errors may not adequately reflect the data.

Shapes of line features are not always well represented by Gaussians. These shapes may be the result of reaction kinematics or of a blending of multiple lines, neither of which is included explicitly in this analysis. The varying shapes of the features are simply approximated in the model by adjusting the width of the Gaussians.

Analysis of Widths

As seen in Table 1, the observed atmospheric gamma-ray line features have widely varying widths (entries containing dashed lines indicate that the apparent width is indeterminate; see detailed discussion of line features in the discussion). There are two possible causes for varying widths:

1) Doppler broadening of the line due to nuclear recoil momentum at the time of deexcitation.

Doppler broadening occurs in atmospheric lines when, after a nuclear reaction, a nuclide undergoes the gamma-ray-emitting transition before ionization losses stop it. We gauge the importance of Doppler broadening as follows.

The mean pathlength traveled before decay is:

$$\lambda = \rho \, v \, \tau$$

Where ρ is the atmospheric density at the altitude where the reaction occurs, v is the recoil velocity, and τ is the mean lifetime of the excited state. (Time dilation is negligible.)

An upper limit on transition pathlength in the upper atmosphere may be calculated. We use the atmospheric density at sea level (about 50 times greater than at 20 g cm^{-2}). We take 100 ps as the upper limit of the mean lifetime of a level. Finally we assume that v = c, which is several times higher than the average nuclear recoil energy. The upper limit on pathlength is then:

$$\lambda << 5 \times 10^{-4} \text{ g cm}^{-2}.$$

This upper limit on the pathlength a nucleus will travel prior to deexcitation is substantially smaller than the typical range of a recoil product (about 10^{-3} g cm^{-2}).

We conclude from the discussion above that all of the atmospheric lines with the exception of the 511 keV annihilation line, which has a different origin, will suffer the maximum possible amount of Doppler broadening. As most of them are likely to be produced by (n,nγ) interactions on N and O, we expect a smooth increase in the Doppler broadening of individual lines proportional to energy. Broadening may vary in reactions where additional neutrons and charged particles are emitted.

The measured widths are in general about 4% of the line energy. For solar flares Murphy [private communication] estimates that widths of the Doppler-broadened lines are about 2% of the line energy. The greater widths of the atmospheric lines may in large part be due to the much harder spectrum of atmospheric neutrons, which will impart more momentum to the recoil nucleus. Detailed calculations of the broadening due to reaction kinematics are required.

2) Blending of multiple lines which are not resolved by the detector.

The most striking evidence for such line blending is the line feature at 5.12 MeV. This feature has a width of 550 keV (FWHM) or over 10% of the line energy. Although this feature is presumably dominated by the 8.6 ps transition to ground state of ^{14}N, there are several other likely gamma-ray lines that can contribute (see Table 2).

DISCUSSION

The Origin of Atmospheric Gamma Ray Lines

Our interpretation of the model photon spectrum, presented in the previous section, focuses on identifying the nuclear transitions responsible for the line features and inferring the nuclear reactions which produce these excited levels. The reactions leading to gamma radiation from the atmosphere are initiated primarily by cosmic-ray protons. At the high cutoffs (> 4 GV/c) considered here the protons are predominantly relativistic. They interact in a medium composed almost entirely of ^{14}N and ^{16}O nuclei. (^{40}Ar is ~ 50 times less abundant than ^{16}O.)

Cosmic-ray protons can excite gamma-ray levels in air, directly and indirectly, in at least four distinct ways:

(1) Direct excitation of ^{14}N and ^{16}O nuclei by protons.

Direct excitation of air nuclei is associated with low-energy (E < 100 MeV) proton interactions. Cross sections for these reactions have been reviewed by Ramaty, Kozlovsky, and Lingenfelter [1979]. The strongest lines expected are the 2.313 MeV line from ^{14}N and the 6.129 MeV line from ^{16}O. The vertical geomagnetic cutoff at the SMM orbit is greater than 4 GV/c, hence few low-energy primary protons impinge on the atmosphere. Since low-energy secondary protons are unlikely to

react in air before stopping, we expect only a small contribution to the gamma-ray line intensities from direct-excitation reactions.

(2) Spallation of ^{14}N and ^{16}O nuclei by protons resulting in excited product nuclei.

The most common product of proton spallation in the atmosphere is ^{12}C produced in the reaction $^{14}N(p,p\alpha)^{12}C$ [Silberberg and Tsao, 1973]. ^{12}C has a single excited state at 4.438 MeV. Other peripheral reaction products such as ^{13}C, ^{15}O, and ^{15}N emit lines at several energies. These peripheral reactions, and the ^{12}C production, dominate the total proton spallation cross section at energies below 50 MeV. At higher energies many reaction channels are possible. In particular, semi-empirical formulas for high-energy proton reactions [Silberberg and Tsao, 1973] predict lighter particles such as ^{10}B, ^{7}Be, ^{7}Li, and ^{6}Li. Gamma-ray lines from these nuclei are characteristic of high-energy proton spallation reactions [Silberberg, Tsao, and Letaw, 1985].

(3) Inelastic scattering of secondary neutrons.

In addition to light nucleus production, high-energy spallation reactions yield free neutrons. These neutrons go on to interact and cause gamma-ray emission primarily through inelastic reactions of the form $(n,n\gamma)$. These neutrons should be the strongest source of gamma emission as demonstrated by the following argument:

Ramaty, Kozlovsky, and Lingenfelter [1975] have reviewed the neutron-production mechanism in high-energy spallation reactions with C, N, and O. They determined the neutron-production cross section to be ~ 1000 mb compared with a total interaction cross section of ~ 300 mb. These numbers imply a mean neutron multiplicity of more than 3 neutrons per reaction at energies above 1 GeV. From this we can estimate the relative yield of gamma rays. Ling [1975] found that among the most common gamma-ray line production reactions in the atmosphere about 14% of the neutrons react to form $^{11}B^*$(4.445 MeV) which subsequently decays directly to its ground state. Thus for each high-energy proton reaction in the atmosphere about 0.5 photons with E = 4.445 MeV are produced in $(n,\alpha\gamma)$ reactions with ^{14}N.

The indirect production of gamma rays by secondary neutrons may be compared with direct production in spallation reactions. The cross section for production of ^{12}C in air is ~ 50 mb compared with a total interaction cross section of ~ 300 mb. Some of these nuclei are formed in the 4.439 MeV excited state, meaning that $\leq$ 0.16 photons with E = 4.438 MeV are produced in each high-energy proton reaction. This production rate is substantially less than the 0.5 photons from neutron-induced reactions. Other spallation gamma rays occur even less frequently.

Neutron-induced lines should therefore dominate spallation-induced lines in the atmosphere. However, the ^{12}C spallation product should contribute 25% - 35% to the line intensity around 4.44 MeV. Other spallation-induced lines should contribute at somewhat lower

levels to the overall line intensity. Spallation-induced lines may be obscured by neutron-induced lines unless they occur at distinct energies.

(4) Capture of secondary neutrons.

Neutron capture is an additional source of gamma-ray lines. Neutron-induced lines produced in the $(n,X\gamma)$ scattering reactions may be distinguished from neutron-capture lines produced in the (n,γ) reaction. In these two mechanisms both the energy-dependence of the reaction cross sections and the distribution of gamma-ray line intensities differ. Ling [1975] computes the expected intensities of several neutron-capture lines originating in the reaction $^{14}N(n,\gamma)^{15}N$. The strongest of these lines occur in transitions from the 10.83 MeV level and are one to two orders of magnitude weaker than the strongest neutron inelastic scattering lines.

Comparison of Relative Line Intensities with Theoretical Calculations

The intensities of gamma-ray lines from the atmosphere were estimated by Ling [1975] using a semi-empirical model. His model assumes that gamma-ray lines (other than at 511 keV) result from neutron capture and inelastic scattering reactions on ^{14}N and ^{16}O. (As discussed above, neutron inelastic scattering is expected to be the dominant source of atmospheric gamma-ray line energy.) A source

function at zero depth is defined as the rate of gamma-ray production in a medium of atmospheric composition by a spectrum of neutrons having a shape consistent with observations. Ling's model relies on the available cross sections for gamma-ray production in neutron interactions and emission is assumed to be isotropic. The source function at any arbitrary atmospheric depth is modeled using the measured growth curve of neutrons. The estimated gamma-ray line intensities as a function of angle are then obtained by integrating the source function over the atmosphere, and including attenuation. Ling's model does not predict the widths of atmospheric gamma-ray lines.

Figure 8 shows a comparison of the relative intensities obtained from our fits (see Table 1) and Ling's predictions. For purposes of comparison, both samples were first normalized using the mean of the 1.63 MeV and 6.1 MeV intensities. Ling provides upper and lower limits of line intensities (shown as boxes in the Figure) which typically differ by an order of magnitude. The absence of neutron cross sections above 17 MeV prevented him from obtaining a more precise determination of the intensity. The height of each box spans the measured FWHM of line features and the energy range over which features were summed to compare with Ling's predictions. Reasonable agreement is found within the broad limits of this comparison except in one case. The relative intensity of the feature near 3.03 MeV appears to be more than an order of magnitude more intense than estimated by Ling. This discrepancy is discussed later and may in part be due to inadequacies in the model used in fitting the data.

Heavy vertical lines in Figure 8 are estimates of the relative atmospheric line intensities which we derived from Reedy's [1978] calculation of lunar gamma-ray lines. Lunar soil is composed primarily of oxygen, but contains some nitrogen. Relative atmospheric gamma-ray line intensities may therefore be derived from Reedy's tables by adjusting for the difference in composition. Reedy adopted a neutron spectrum having the same shape as the atmospheric neutron spectrum; he also estimated the high-energy (E > 17 MeV) neutron cross sections. This modified version of Reedy's calculations is also in reasonable agreement with our measurements except for the feature at 3.03 MeV.

Discussion of Individual Line Features

In the following we provide a detailed discussion of the observed individual line features in the light of the analysis above. We compare these observations with the work of Ling [1975], Reedy [1978], and a compilation of gamma-ray lines observed in nuclear reactions of light nuclei extracted from De Meijer et al. [1974] and summarized in Table 2. (Two lines from transitions from the 11.06 MeV state in ^{16}O which were mentioned by Ling have been added.) About half of the lines listed in Table 2 are strong enough that they were included in Ling's [1975] modeling of neutron-induced reactions in the atmosphere and/or Murphy's [1985] modeling of proton-induced reactions in solar flares [Ramaty, Kozlovsky, and Lingenfelter, 1979]. These are designated by the letters 'L' or 'R' in the Table. The reaction cross sections leading to most of these gamma rays are unknown. In general,

more than one significant transition could contribute to each line feature identified in our analysis.

0.4 - 0.6 MeV

The 511 keV line is only 2.3 keV (FWHM) wide [Mahoney, Ling, and Jacobson, 1981], which is too narrow to be resolved by our instrument. It is also more than 5 times more intense than the strongest nuclear line observed near 4.45 MeV. The fit is not adequate below the peak due to the strong flat continuum which we attribute to Compton scattering in the atmosphere. The effect of Compton scattering has been introduced in the one-dimensional slab approximation using an inverse scattering mean free path of $0.0636E^{-0.5}$ cm^2 g^{-1}. The fit to the data is improved by introducing a 21 ± 1 g cm^{-2} slab of atmosphere between the source and detector (Figure 3). Such an average scattering depth is reasonable for photons primarily resulting from electromagnetic showers. Compton scattering does not affect the shape of the spectrum above 1 MeV, but does increase the inferred line and background intensities within the atmosphere as predicted by the energy-dependent mean free path.

0.7 - 0.8 MeV

A feature at 0.735 MeV is necessary to fit the data. Ling predicts a line from the ^{14}N transition from 5.833 MeV to 5.106 MeV at nearly this energy (see Figure 3).

0.8 - 1.5 MeV

No lines of atmospheric origin were identified in this interval. Residuals of the ^{60}Co calibration lines at 1.333 MeV and 1.165 MeV can be seen in Figure 4 lying below the fit to the data. These residual intensities are approximately 1% of their value in the uncorrected 'earth-viewing' spectrum. Residuals from incomplete subtraction of other strong intrinsic background lines from the detector and are also apparent in this interval.

1.5 - 1.8 MeV

The spectrum in this interval is fitted by a single line at 1.63 MeV with a 65 keV (FWHM) width. This feature can be attributed to a line from the transition of ^{14}N from 3.945 to 2.313 MeV.

1.8 - 2.2 MeV

A strong line feature is observed in this interval at 2.14 MeV. A line from ^{11}B at the measured relative intensity is expected at

2.124 MeV according to Ling and the modified calculation of Reedy. Both this feature and the line at 4.450 MeV can be attributed to the $^{14}N(n,\alpha)^{11}B^*$ reaction. Doppler broadening of these features is expected to be greater than in the $(n,n\gamma)$ reactions, such as those which produce the 1.63 and 2.32 MeV lines, due to the emission of an α particle. This excess broadening seems to be observed. We would also expect the width of the lower-energy ^{11}B line to be narrower than the higher-energy line because the broadening should scale linearly with energy.

A weak feature at 1.90 MeV was inserted manually to make up for a slight deficiency in counts. It may be due to the ^{11}C transition at 1.995 MeV.

2.2 - 2.4 MeV

The feature at 2.32 MeV is well-fitted by a Gaussian. Its measured energy is within 1.3 standard deviations of that expected for the ^{14}N line at 2.313 MeV and its relative intensity is about a factor of two below Ling's predictions (see Figure 8).

2.4 - 2.9 MeV

It is clear from Figure 5 that the model used to fit does not adequately fit the apparent line feature at 2.78 MeV. The formal parameters obtained for this feature are given in Table 1. The relative intensity of the feature at 2.78 MeV is consistent with

Ling's estimate for the 8.872 MeV to 6.131 MeV transition in ^{16}O, although its fitted central energy is about 3 standard deviations high. In addition the fitted width of the feature is high. Inspection of Figure 5 suggests that the width of the line should be significantly narrower than given by the model and that the line energy should be lower. This would bring the parameters in better agreement with the supposition that this feature is primarily due to the 2.741 MeV line from ^{16}O.

A possible line feature at 2.54 MeV was inserted manually to make up for a deficiency of counts in the region. Possible transitions at this energy are indicated in Table 2. We also note that a residual feature from the sum peak of the ^{60}Co calibration lines will also appear at this energy.

2.9 - 3.2 MeV

There is only a weak visual indication of an enhancement in this interval. It was fitted by a broad feature centered near 3.03 MeV, although inspection of Figure 5 suggests that the width of the line should be significantly narrower than given by the model. The poor fit may be due insufficient strength in the underlying continuum. This uncertainty in the fit is reflected by the '?' in Table 1. Ling predicts a ^{13}C line (from an ^{16}O reaction) in this interval, whose relative intensity is more than a factor of 10 weaker than the intensity listed in the Table.

3.2 - 3.5 MeV

The dominant feature in this region is a broad peak at 3.40 MeV whose 270 keV (FWHM) suggests that it is a blend of several atmospheric lines. Ling only lists a single line from ^{14}N in this energy interval at no more than half the measured intensity. Candidates for other lines are shown in Table 2.

3.5 - 3.8 MeV

An excellent fit to a feature at 3.69 MeV is found in this interval. A line from ^{13}C is expected in this energy interval at 3.684 MeV.

3.8 - 4.0 MeV

An excellent fit to a feature at 3.91 MeV is found in this interval. Lines from ^{13}C and ^{14}N of about equal strength and separated by only 31 keV are expected in this interval.

4.0 - 4.3 MeV

A weak feature at 4.19 MeV was required by the fitting routine to fill in the energy interval between 4.0 MeV and 4.3 MeV. There is marginal visual indication of a such peak. The width could not be determined. Ling lists a weak feature from the decay of the 11.06 MeV level of ^{16}O at 4.140 MeV.

4.3 - 4.6 MeV

The feature at 4.45 MeV is the strongest nuclear line feature from the atmosphere. Ling attributes it to production of the first excited state of ^{11}B in the reaction $^{14}N(n,\alpha)^{11}B$ with subsequent decay to its ground state yielding a line at 4.443 MeV. The spallation reaction product, ^{12}C, emits a line at 4.438 MeV and could contribute about 1/3 of the line intensity in this region.

4.6 - 5.4 MeV

An extremely broad feature at 5.12 MeV is the second strongest nuclear line feature from the atmosphere. Ling finds that the 5.105 MeV transition of ^{14}N to its ground state should be the strongest line in this region. It is the fourth most intense nuclear line on his list, behind lines at 1.632 MeV and 2.313 MeV from ^{14}N and 6.129 MeV from ^{16}O. The measured width of this feature is 550 keV (FWHM), by far the largest among the features we have identified. It therefore is likely that it contains a blend of lines, including those from the two lowest levels of ^{15}O and ^{15}N to the ground state.

5.4 - 5.9 MeV

The line structure in this interval is poorly represented by a single Gaussian. We have fitted it using two Gaussians centered at 5.85 MeV and 5.61 MeV, corresponding to expected ^{14}N gamma rays at 5.832 MeV and 5.690 MeV. The lines overlap strongly. This overlap introduces uncertainty into the line intensities and obscures measurement of the individual widths. The energy of the 5.611 MeV line

is several standard deviations lower than expected and may indicate additional blending from the ^{11}C line at 5.513 MeV.

5.9 - 6.3 MeV

The spectrum in this region is well approximated by a Gaussian-shaped line centered at 6.178 ± 0.006 MeV with width 220 keV (FWHM). While it is expected that this feature would be dominated by the 6.129 MeV line from ^{16}O, the measured energy is almost exactly equal to the 6.176 MeV line from ^{15}O. This could indicate contributions from other transitions listed in Table 2. Another explanation for the difference in energy is an error in the calibration of the instrument. Further investigation of this possibility is underway.

6.3 - 6.6 MeV

The feature in this interval has been modeled with a single Gaussian centered at 6.46 MeV. This feature is relatively weak. Lines at 6.322 MeV from ^{15}N and at 6.442 MeV from ^{14}N are expected to occur in this interval. Two lines from ^{11}C may also contribute.

6.6 - 7.2 MeV

The spectrum is well represented in this interval by a Gaussian feature centered at 6.927 ± 0.009 MeV. The feature appears to be wider than expected from Doppler broadening of a single line. Ling lists four lines of roughly equal strength from ^{16}O, ^{14}N, and ^{14}C that may contribute in this region.

7.2 - 8.5 MeV

The fit was not improved by introducing lines in this region.

CONCLUSIONS

In this paper we have presented measurements of the atmospheric gamma-ray line features from 300 keV to 8.5 MeV. Twenty features have been identified and estimates of their center energies, widths, and intensities are reported. These spectral parameters were determined within a model based on a power-law continuum with Gaussian features superimposed.

The assumed power-law continuum background was found to have an index of α = -1.16 (photon spectrum). The precise nature of the continuum is obscured by many superimposed lines and there is a suggestion that this simple power-law representation may not be adequate to fit the observations (*i.e., in* the interval 2.4 MeV to 3.2 MeV interval). The power-law index of the continuum in the count spectrum has a value of β = -1.63, which is somewhat steeper than the value of β = -1.4 reported earlier by Peterson, Schwartz, and Ling [1973]. Our continuum is steeper because we have separated the nuclear lines from the background.

The observed continuum below 511 keV substantially exceeds our power-law background model. This is attributed to Compton scattering of the 511 keV photons. A calculation based on that assumption yields the average production depth in the atmosphere (slab-equivalent) of 21 $\pm$ 1 g cm^{-2}. This is not necessarily the average production depth of the higher energy nuclear lines because different production mechanisms are expected.

Our data support the theoretical prediction that atmospheric gamma-ray lines are produced predominantly by secondary-neutron interactions with ^{14}N and ^{16}O. Ling's [1975] atmospheric model and our modification of Reedy's [1978] lunar model make order-of-magnitude predictions of relative line intensities which are generally in fair agreement with our observations. Their predictions, and hence a detailed assessment of the theoretical models, are limited by cross-section uncertainties. The widths of the line features are in qualitative agreement with predictions based on reaction kinematics.

The present analysis does little to clarify the contribution of spallation reactions and other mechanisms to the overall atmospheric gamma-ray line flux. A possible 25% - 35% contribution from the ^{12}C spallation product at 4.438 MeV is obscured by neutron-induced lines at the same energy and at 4.443 MeV (from ^{11}B). The direct excitation lines from ^{16}O at 6.129 MeV and from ^{14}N at 2.313 MeV are produced by neutron, as well as proton, reactions. Another possible spallation line from ^{15}O at 6.176 MeV is confused with the nearby ^{16}O line. We do not observe strong signatures of high-energy spallation lines (^{7}Li, ^{6}Li, etc.) or neutron capture reactions (primarily transitions from the 10.83 MeV level of ^{15}N).

Considerable improvement in our understanding of the mechanisms responsible for atmospheric gamma-ray emission can be anticipated from in-depth modeling. Many features of a complete model, such as the molecular composition of the atmosphere, the atmospheric intensities of neutron and protons, the kinematics of nuclear interactions, the

geometry of the atmosphere, and photon attenuation rates, are well known. Other features which are not so well known, such as energy dependence of the cross sections, may be constrained by the excellent statistics of the atmospheric spectrum. This modeling would be of collateral benefit to other astrophysical studies of gamma-ray line production, such as in solar flares [Murphy, 1985], because it provides an overall, independent test of techniques.

ACKNOWLEDGEMENTS

We appreciate discussions with Ron Murphy, Jim Ling, and C.H. Tsao on topics closely related to this research. We thank Dan Messina for assistance in processing the data. This work was supported by NASA contract S-14513-D at NRL and grant NAS 5-28609 at UNH, and by BMFT contract 010k 017-za/ws/wrk at MPE.

REFERENCES

De Meijer, R.J., Plendl, H.S., and Holub, R., Tables for Reaction Gamma-Ray Spectroscopy, Part I: A=6 to A=20, Atomic Data and Nuclear Data Tables, 13, 1-33, 1974.

Dunphy, P.P., Forrest, D.J., Chupp, E.L., Cherry, M.L., and Ryan, J.M., Limit on a Galactic 6.13 MeV γ-Ray Line, Ap. J., 244, 1081-1086, 1981.

Forrest, D.J. et al., The Gamma Ray Spectrometer for the Solar Maximum Mission, Solar Phys., 65, 15-23, 1980.

Lederer, C.M. and Shirley, V.S., Table of Isotopes, J. Wiley and Sons, New York, 1978.

Ling, J.C., A Semiempirical Model for Atmospheric Gamma Rays from 0.3 to 10 MeV at 40° Geomagnetic Latitude, J. Geophys. Res., 80, 3241-3252, 1975.

Lockwood, J.A., Hsieh, L., Frilling, L., Chen, C., and Swartz, D., Atmospheric Neutron and Gamma Ray Fluxes and Energy Spectra, J. Geophys. Res., 84, 1402-1408, 1979.

Mahoney, W.A., Ling, J.C., and Jacobson, A.S., HEAO-3 Measurements of the Atmospheric Positron Annihilation Line, J. Geophys. Res., 86, 11098-11104, 1981.

Murphy, R., Gamma Rays and Neutrons from Solar Flares, Ph.D. Dissertation, NASA/Goddard Space Flight Center, 1985.

Peterson, L.E., Schwartz, D.A., and Ling, J.C., Spectrum of Atmospheric Gamma Rays to 10 MeV at Lambda = 40°, J. Geophys. Res., 78, 7942-7958, 1973.

Ramaty, R., Kozlovsky, B., and Lingenfelter, R.E., Solar Gamma Rays, Space Sci. Rev., 18, 341-388, 1975.

Ramaty, R., Kozlovsky, B., and Lingenfelter, R.E., Nuclear Gamma-Rays from Energetic Particle Interactions, Ap. J. Suppl., 40, 487-526, 1979.

Reedy, R.C., Planetary Gamma Ray Spectroscopy, in: Gamma Ray Spectroscopy in Astrophysics, ed. T.L. Cline and R. Ramaty, NASA Technical Memorandum 79619, 1978.

Ryan, J.M, Dayton, B., Moon, S.H., Wilson, R.B., Zych, A.D., and White, S.R., Atmospheric Angle and Energy Distributions from 2 to 25 MeV, J. Geophys. Res., 82, 3593-3601, 1977.

Share, G.H., Kinzer, R.L., Kurfess, J.D., Forrest, D.J., Chupp, E.L., and Rieger, E., Detection of Galactic ^{26}Al Gamma Radiation by the SMM Spectrometer, Ap. J. (Letters), 292, L61-L65, 1985.

Share, G.H., Kinzer, R.L., Kurfess, J.D., Messina, D.C., Purcell, W.R., Chupp, E.L., Forrest, D.J., and Reppin, C., SMM Detection of Diffuse Galactic 511 keV Annihilation Radiation (submitted to Ap. J.).

Silberberg, R., and Tsao, C.H., Partial Cross Sections in High-Energy Nuclear Reactions, and Astrophysical Applications, Ap. J. Suppl., 25, 315-368, 1973.

Silberberg, R., Tsao, C.H., and Letaw, J.R., Gamma-Ray Line Production from Cosmic-Ray Spallation Reactions, Proc. 19th Internat. Cosmic Ray Conf. (La Jolla), 1, 369-372, 1985.

Willett, J.B., Ling, J.C., Mahoney, W.A., and Jacobson, A.S., Detection of 6.13 MeV Gamma Rays Within and at the Top of the Atmosphere, Ap. J., 234, 753-760, 1979.

TABLE 1: Observed Atmospheric Gamma Ray Line Features
(Model Fit Parameters [a])

Energy (MeV)	Relative Intensity [b]	Width (keV (FWHM))	
0.511 ± .001	36.5 ± .7	----	
0.735 ± .003	1.06 ± .06	45 ± 10	
1.641 ± .006	0.76 ± .09	65 ± 25	
1.90	0.45	----	
2.138 ± .010	1.79 ± .22	140 ± 30	
2.321 ± .006	1.99 ± .21	80 ± 20	
2.54	0.40	----	
2.778 ± .011	1.20 ± .26	230 ± 40	?
3.027 ± .016	1.63 ± .24	300 ± 30	?
3.402 ± .024	1.51 ± .34	270 ± 80	
3.693 ± .018	1.83 ± .63	140 ± 70	
3.909 ± .024	1.73 ± .48	150 ± 60	
4.190 ± .020	0.75 ± .08	----	
4.450 ± .002	5.87 ± .09	180 ± 10	
5.124 ± .008	4.17 ± .09	550 ± 25	
5.611 ± .011	0.69 ± .11	----	
5.848 ± .018	0.57 ± .10	----	
6.178 ± .006	3.28 ± .11	220 ± 15	
6.465 ± .016	0.87 ± .10	160 ± 30	
6.927 ± .009	2.65 ± .09	400 ± 25	

[a] The parameters and uncertainties listed in this table are based on the assumed model. Systematic uncertainties due to the choice of model are not included, e.g., for certain features, the model actually does not fit the data as well as desired. We specify these features by '?' to the right of the entry and discuss the fits in greater depth in the text.

[b] The reported intensities are in units of (10^{-3} photons cm^{-2} s^{-1}) at the detector. Angular dependence of the atmospheric spectrum and detector response is not accounted for in this measurement. Reported intensities approximate the absolute disk average intensity, but are about 50% (25% for the 0.511 MeV line) lower because of the subtraction technique used to remove radioactive background lines.

TABLE 2: Reaction Gamma Rays from ^{14}N and ^{16}O

Energy Range (MeV)	Energy (MeV)	Product Nuclide & Transition (MeV)	Note [a]	Observed Energy (MeV)
0.7-0.8	0.717	^{10}B (0.717 - g.s.)	R	0.735
	0.727	^{14}N (5.833 - 5.106)	L	
0.8-1.5	0.808	^{14}C (6.901 - 6.093)	-	(NONE)
	0.953	^{12}B (0.953 - g.s.)	-	
	0.975	^{8}Li(0.975 - g.s.)	-	
	1.023	^{10}B (1.740 - 0.717)	R	
	1.248	^{14}C (7.341 - 6.093)	-	
	1.437	^{10}B (2.154 - 0.717)	-	
1.5-1.8	1.617	^{15}O (6.859 - 5.242)	-	1.64
	1.632	^{14}N (3.945 - 2.313)	RL	
	1.668	^{12}B (2.621 - 0.953)	-	
	1.674	^{12}B (1.674 - g.s.)	-	
1.8-2.2	1.884	^{15}N (7.155 - 5.271)	-	2.14
	1.995	^{11}C (1.995 - g.s.)	R	
	2.000	^{15}N (9.155 - 7.155)	-	
	2.034	^{15}O (7.276 - 5.242)	-	
	2.124	^{11}B (2.124 - g.s.)	RL	
	2.154	^{10}B (2.154 - g.s.)	-	
	2.190	^{16}O(11.060 - 8.872)	L	
2.2-2.4	2.295	^{15}N (7.566 - 5.271)	-	2.32
	2.298	^{11}B (6.743 - 4.444)	-	
	2.313	^{14}N (2.313 - g.s.)	RL	
2.4-2.9	2.593	^{10}Be(5.959 - 3.366)	-	2.78
	2.691	^{9}Li(2.691 - g.s.)	-	
	2.723	^{12}B (2.723 - g.s.)	-	
	2.741	^{16}O (8.872 - 6.131)	RL	
	2.867	^{10}B (3.585 - 0.717)	-	
	2.896	^{10}Be(6.262 - 3.366)	-	
2.9-3.2	3.086	^{13}C (3.086 - g.s.)	L	3.03
3.2-3.5	3.305	^{15}N (8.576 - 5.271)	-	3.40
	3.359	^{10}C (3.360 - g.s.)	-	
	3.365	^{10}Be(3.366 - g.s.)	-	
	3.378	^{14}N (5.691 - 2.313)	L	
	3.483	^{13}B (3.483 - g.s.)	-	

3.5-3.8	3.534	^{13}B (3.535 - g.s.)	-	3.69
	3.561	^{6}Li(3.562 - g.s.)	-	
	3.684	^{13}C (3.684 - g.s.)	RL	
	3.711	^{13}B (3.712 - g.s.)	-	
3.8-4.0	3.853	^{13}C (3.854 - g.s.)	RL	3.91
	3.884	^{14}N (6.198 - 2.313)	L	
4.0-4.3	4.131	^{13}B (4.132 - g.s.)	-	4.19
	4.140	^{16}O(11.060 - 6.919)	L	
4.3-4.6	4.304	^{11}C (4.305 - g.s.)	-	4.45
	4.343	^{11}C (6.339 - 1.995)	-	
	4.438	^{12}C (4.439 - g.s.)	RL	
	4.443	^{11}B (4.444 - g.s.)	RL	
4.6-5.4	4.667	^{11}B (6.793 - 2.124)	-	5.12
	4.793	^{11}C (4.794 - g.s.)	-	
	4.912	^{14}N (4.913 - g.s.)	L	
	5.018	^{11}B (5.019 - g.s.)	-	
	5.105	^{14}N (5.106 - g.s.)	RL	
	5.180	^{15}O (5.181 - g.s.)	R	
	5.240	^{15}O (5.242 - g.s.)	R	
	5.270	^{15}N (5.271 - g.s.)	RL	
	5.298	^{15}N (5.299 - g.s.)	R	
5.4-5.9	5.513	^{11}C (7.509 - 1.995)	-	5.61
	5.690	^{14}N (5.691 - g.s.)	L	5.85
	5.832	^{14}N (5.833 - g.s.)	L	
	5.870	^{11}B (7.996 - 2.124)	-	
5.9-6.3	5.958	^{10}Be(5.960 - g.s.)	-	6.18
	6.092	^{14}C (6.093 - g.s.)	L	
	6.129	^{16}O (6.131 - g.s.)	RL	
	6.176	^{15}O (6.177 - g.s.)	R	
	6.196	^{14}N (6.198 - g.s.)	-	
6.3-6.6	6.322	^{15}N (6.324 - g.s.)	RL	6.46
	6.337	^{11}C (6.339 - g.s.)	R	
	6.440	^{11}B (8.566 - 2.124)	-	
	6.442	^{14}N (6.444 - g.s.)	L	
	6.478	^{11}C (6.480 - g.s.)	R	

6.6-7.2	6.726	^{14}C (6.728 - g.s.)	L	6.93
	6.741	^{11}B (6.743 - g.s.)	R	
	6.786	^{15}O (6.788 - g.s.)	-	
	6.791	^{11}B (6.793 - g.s.)	R	
	6.904	^{11}C (6.906 - g.s.)	-	
	6.917	^{16}O (6.919 - g.s.)	RL	
	7.010	^{14}C (7.012 - g.s.)	-	
	7.026	^{14}N (7.028 - g.s.)	L	
	7.117	^{16}O (7.119 - g.s.)	RL	
7.2-8.5	7.293	^{11}B (7.296 - g.s.)	-	(NONE)
	7.299	^{15}N (7.301 - g.s.)	RL	
	7.506	^{11}C (7.509 - g.s.)	-	
	7.993	^{11}B (7.996 - g.s.)	-	
	8.310	^{15}N (8.313 - g.s.)	-	

[a] L = Neutron-induced line compiled by Ling [1975]
R = Proton-induced line compiled by Ramaty et al. [1979]
- = Not used in previous astrophysical studies of the Earth's atmosphere and solar flares.

FIGURE CAPTIONS

1. Diagram of the gamma-ray spectrometer on SMM.

2. Mean count-rate spectra from the SMM Gamma Ray Spectrometer accumulated over a three and one-half year period at low (< 11 GV/c) vertical rigidity cutoff. (a) Instrument pointing downward, toward the atmosphere. (b) Difference spectrum obtained by subtracting the upward-pointing spectrum from the downward-pointing spectrum.

3. The 511 keV line from the atmosphere fitted without (a) and with (b) atmospheric Compton scattering. Compton scattering is modeled approximately by a one-dimensional slab, 21 g cm^{-2} thick. Model photon spectra are compared with the observed count spectrum using the detector model.

4. Count spectrum between 0.8 MeV and 2.0 MeV with model fit superimposed.

5. Count spectrum between 2.0 MeV and 4.0 MeV with model fit superimposed.

6. Count spectrum between 4.0 MeV and 6.0 MeV with model fit superimposed.

7. Count spectrum between 6.0 MeV and 8.0 MeV with model fit superimposed.

8. Comparison of the relative intensities of observed atmospheric gamma-ray line features with predictions of Ling [1975] and our revised estimates based on Reedy's [1978] lunar intensities.

FIGURE 1

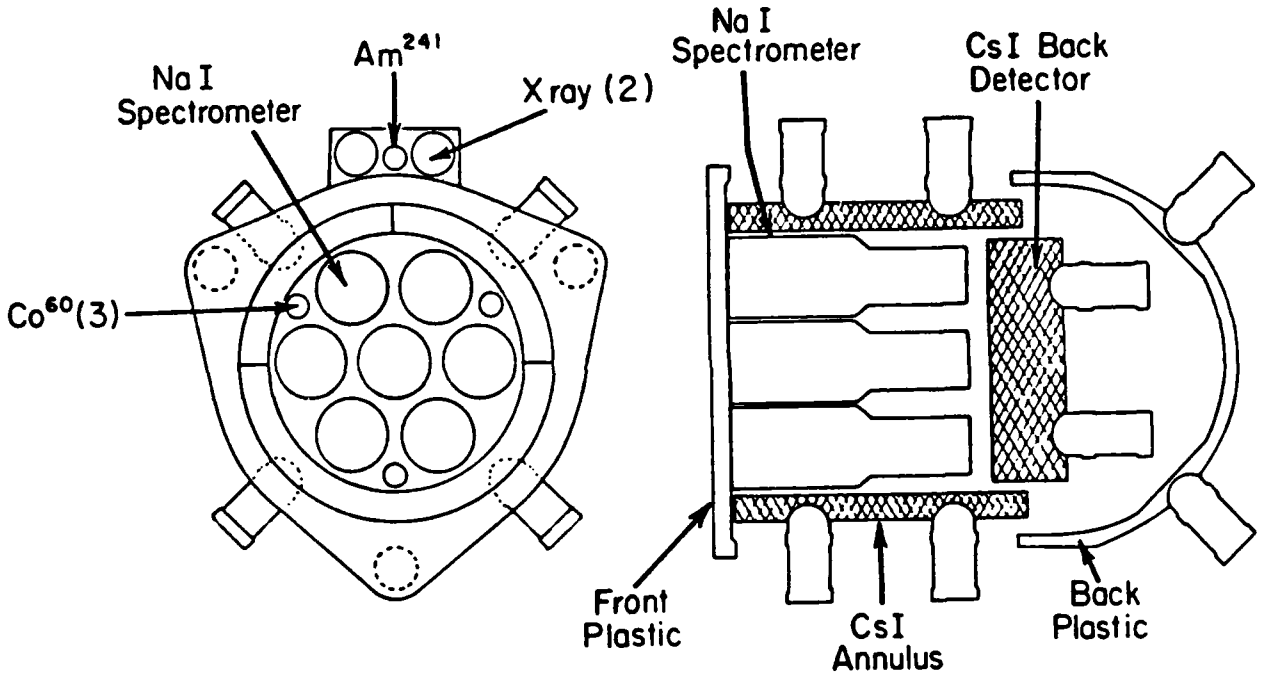
Na I
Spectrometer
Am241
Xray (2)
Co60(3)
Na I
Spectrometer
CsI Back
Detector
Front
Plastic
CsI
Annulus
Back
Plastic

FIGURE 2

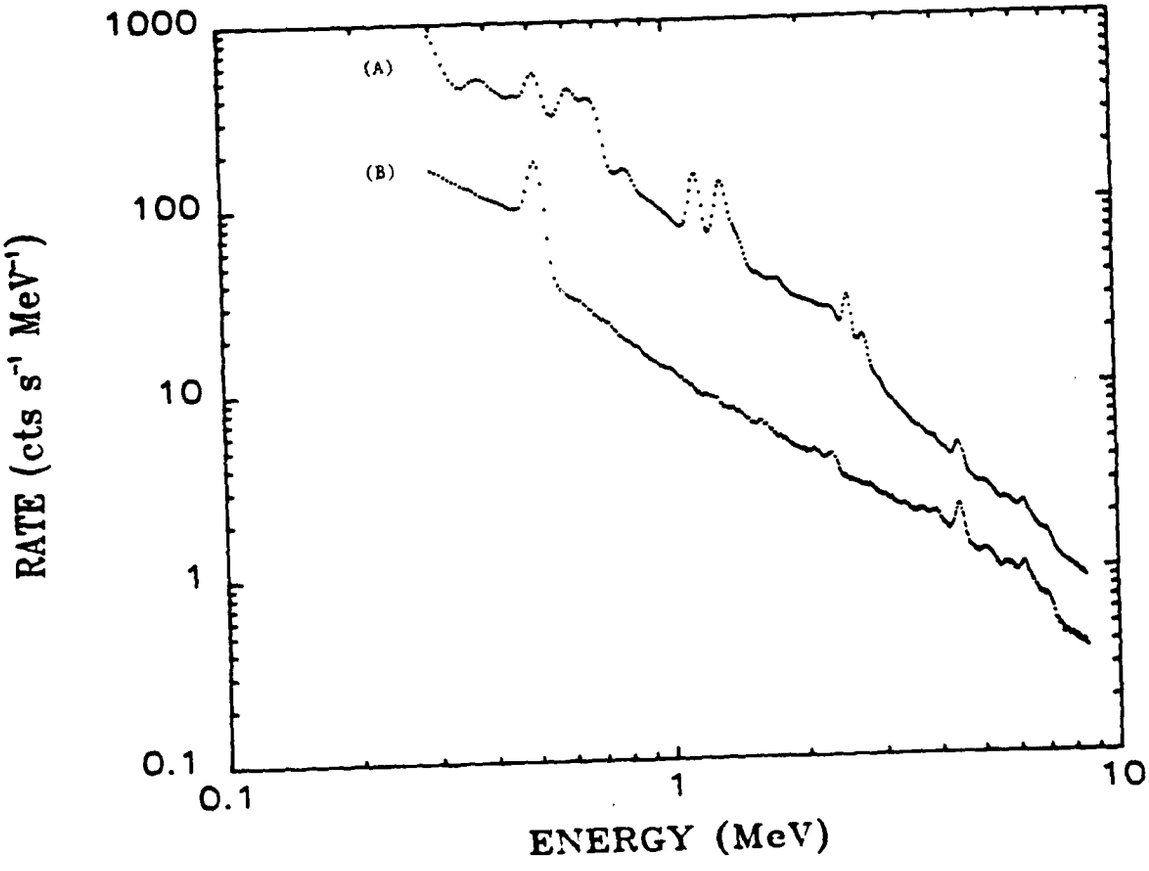

FIGURE 3

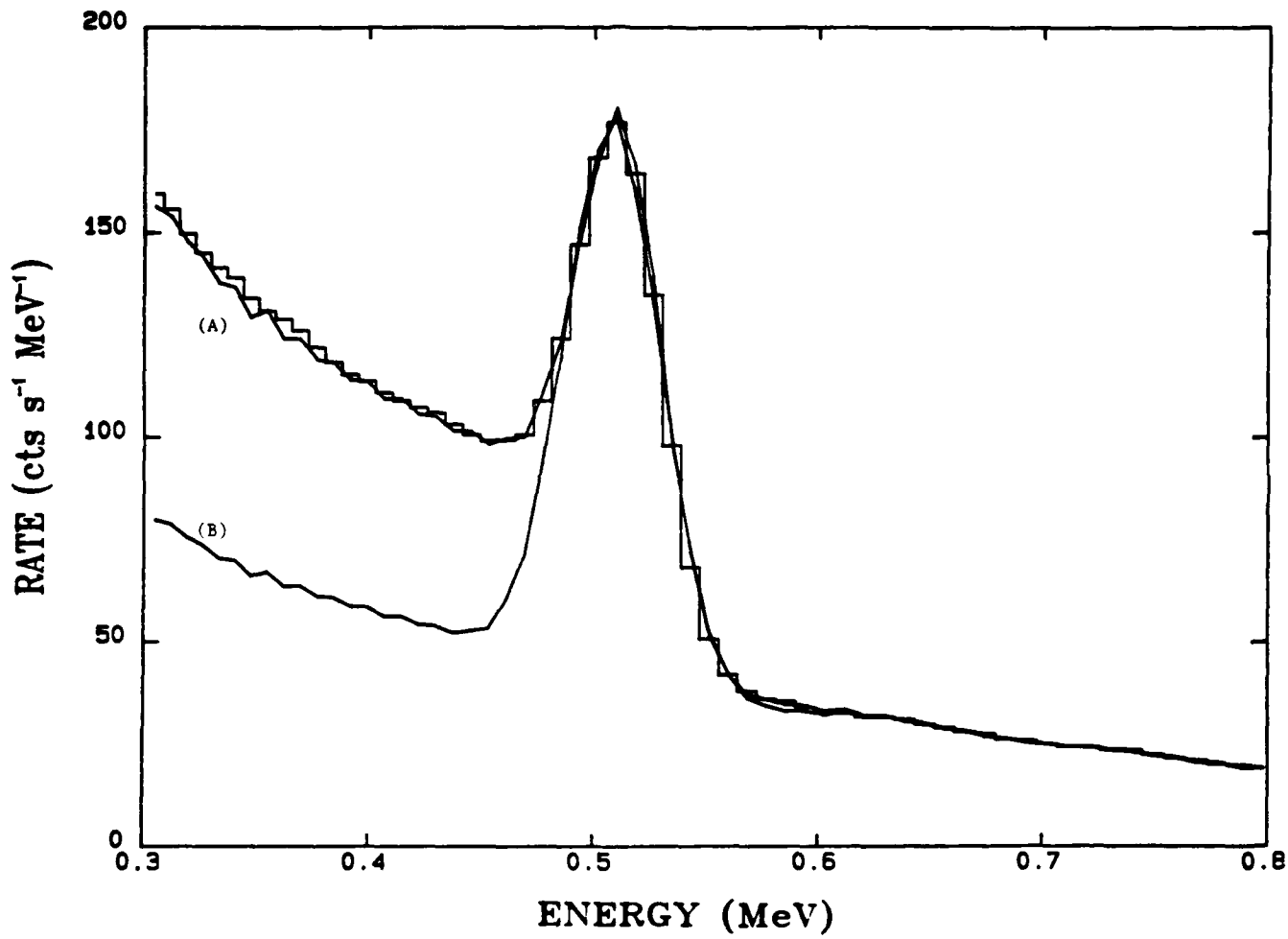

FIGURE 4

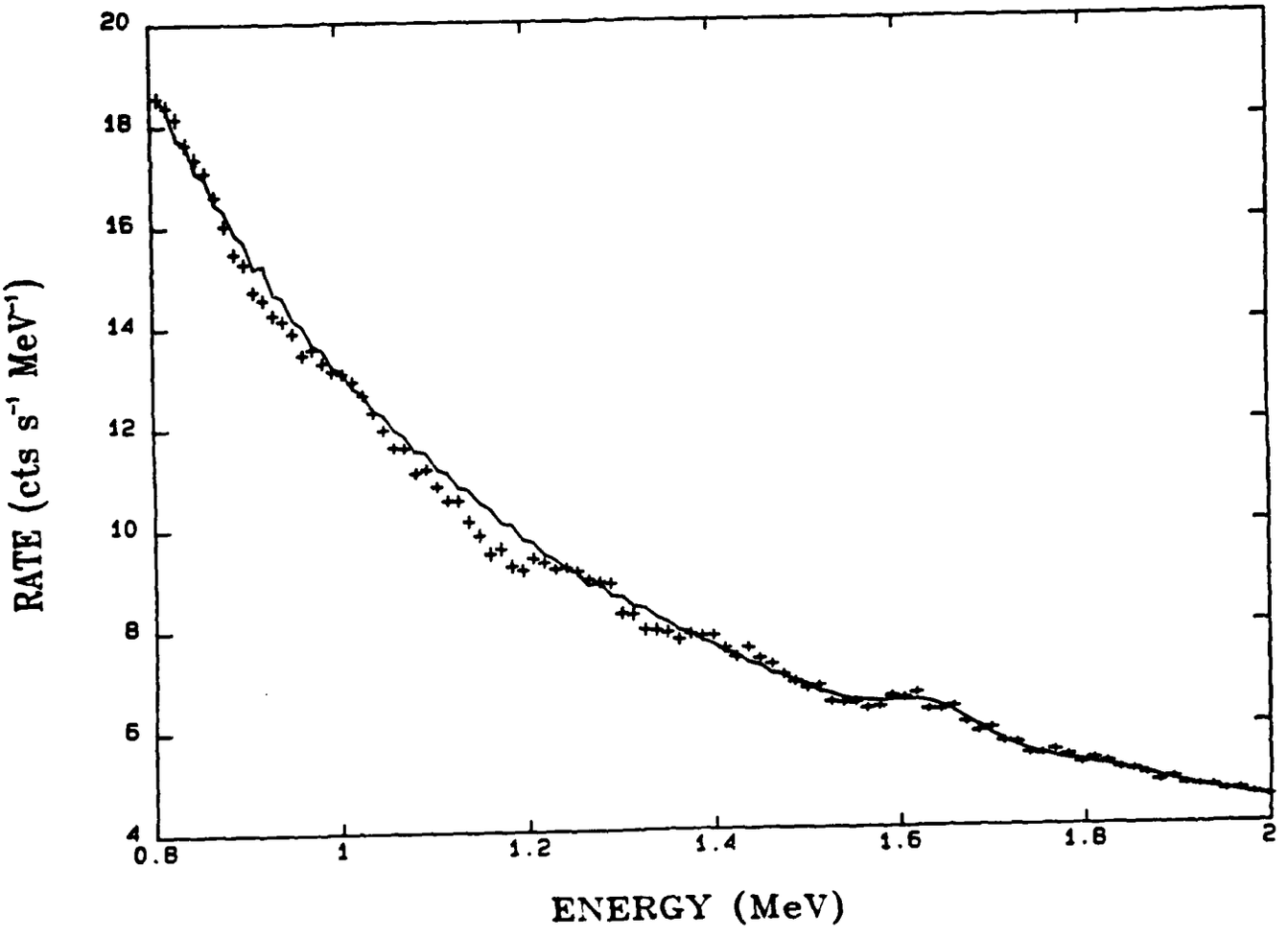

FIGURE 5

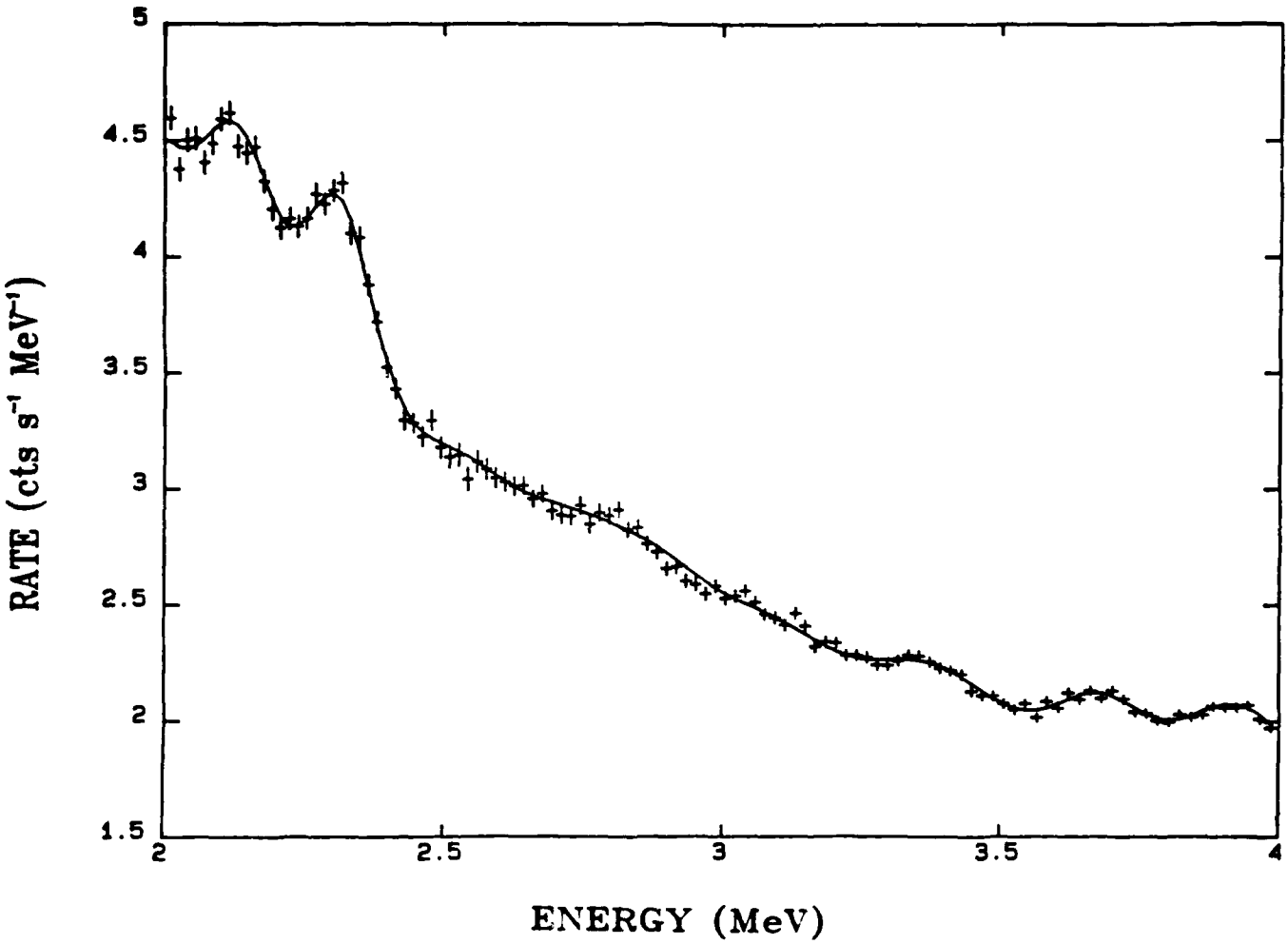

FIGURE 6

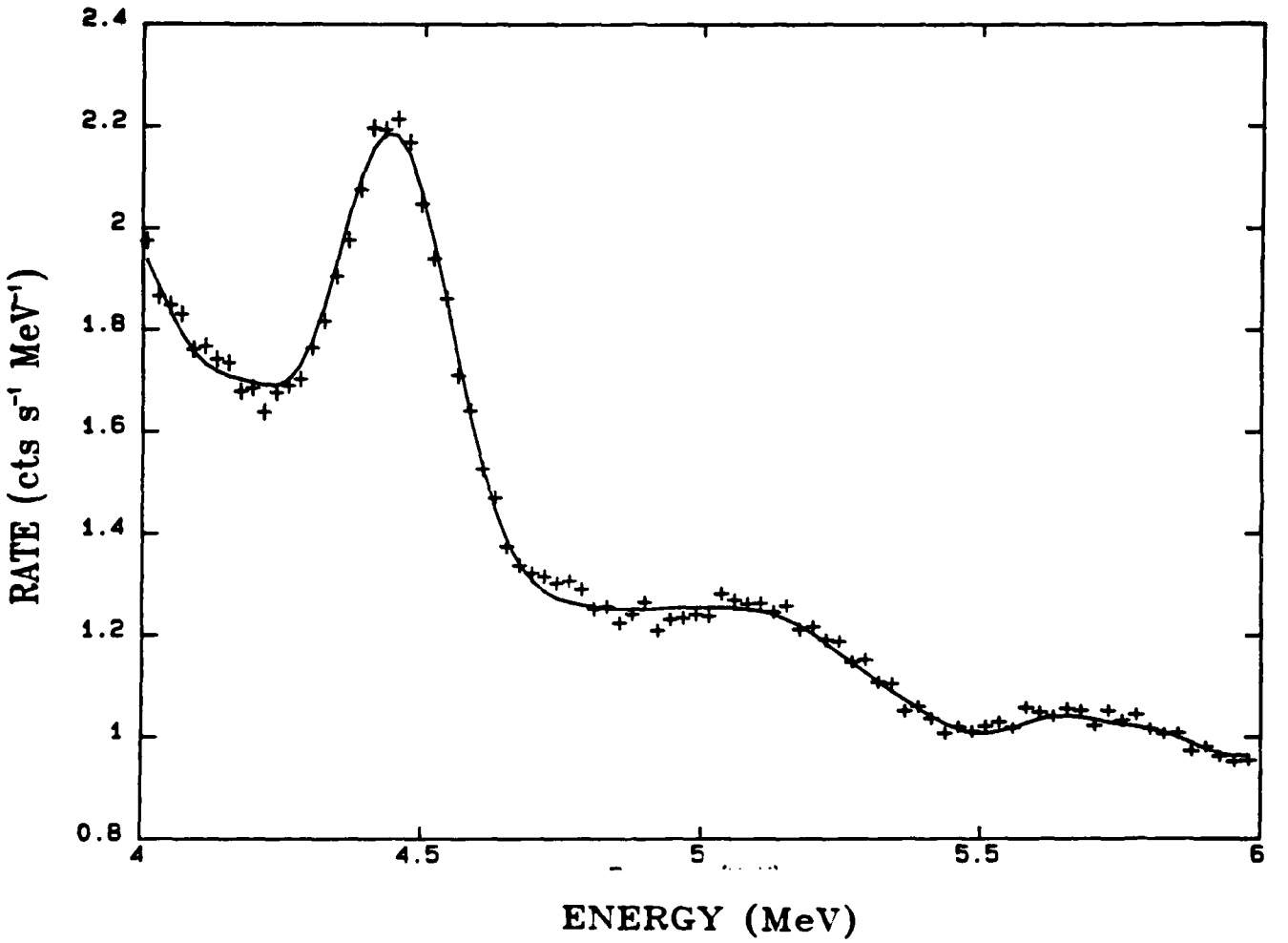

FIGURE 7

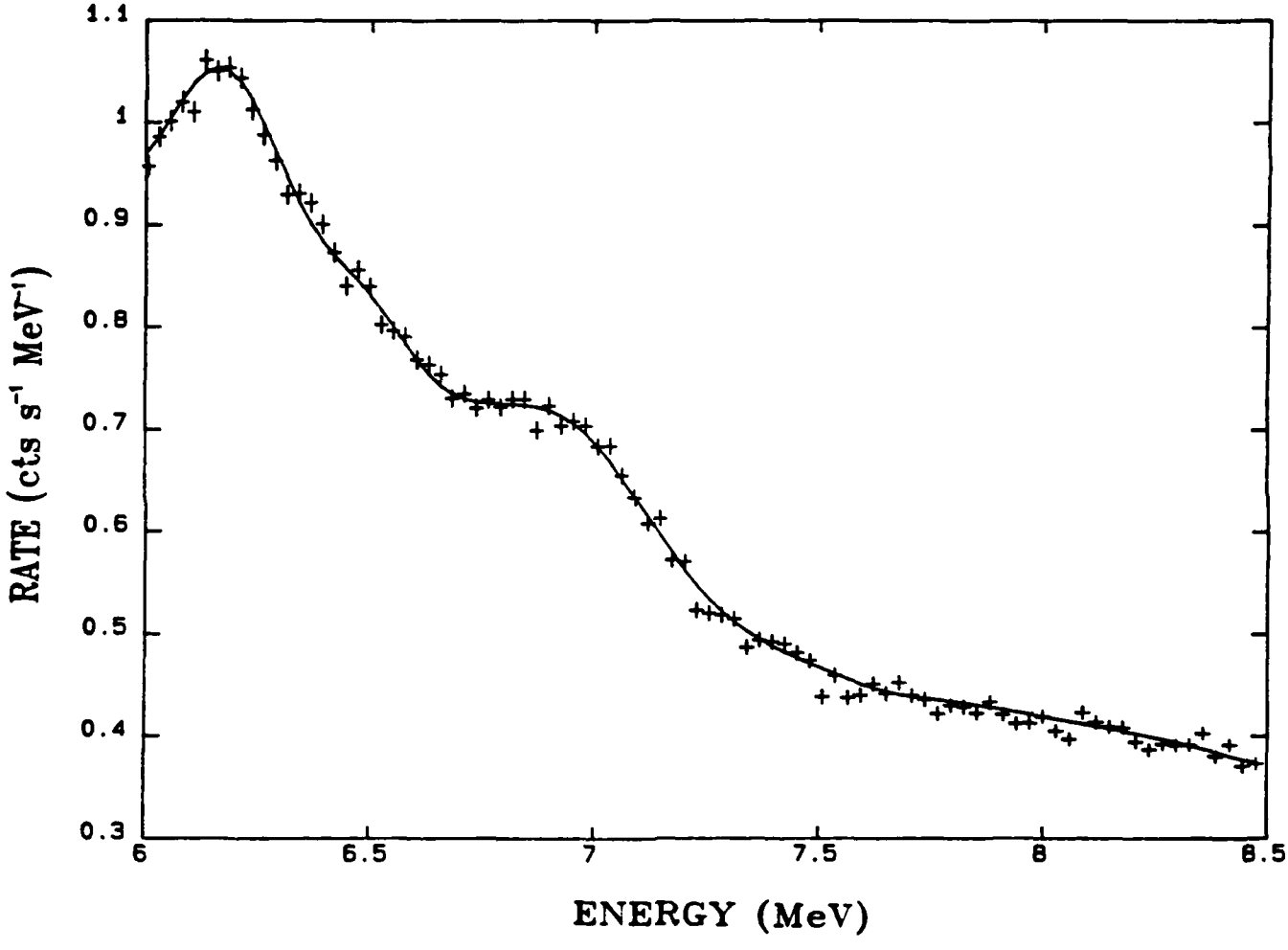

FIGURE 8

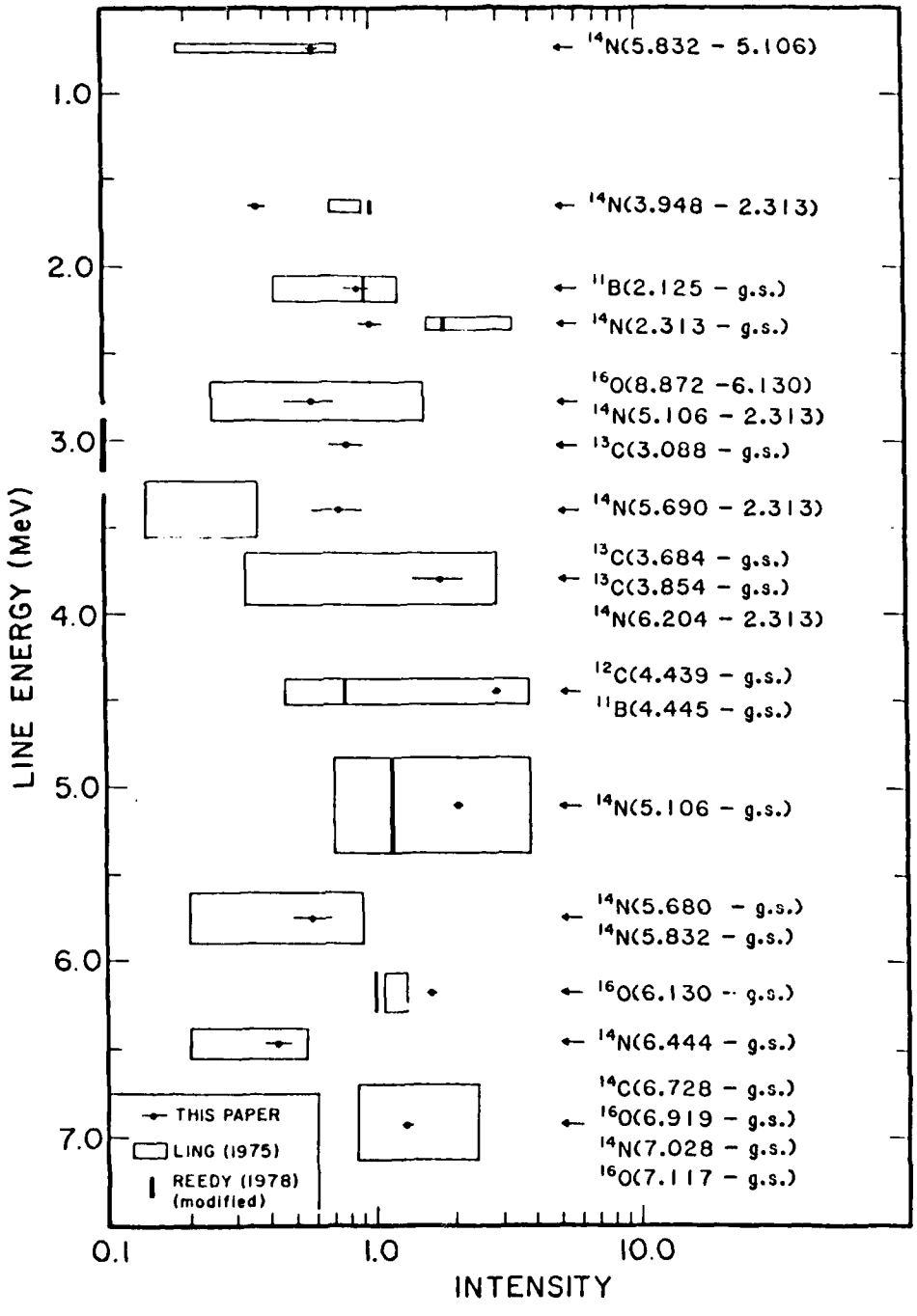

(relative to mean of 1.632 and 6.129 MeV lines)